

Integrated Fourier-Domain Mode-Locked Lasers: Analysis of a Novel Coherent Comb Laser

Martijn J. R. Heck, *Member, IEEE*, and John E. Bowers, *Fellow, IEEE*

Abstract—Fourier-domain (FD) mode locking of integrated laser diode structures is studied theoretically and their application for wavelength division multiplexing (WDM) comb generation for future terabits per second interconnects is discussed. Twenty-five-gigahertz FD mode-locked structures with ring and Mach-Zehnder-based bandpass filters show comb widths of 1.0–1.8 THz, i.e., 40–72 comb lines, but the mode comb is not flat, which increases the mode relative intensity noise (RIN). It is shown that by combining AM and FD mode-locking wide and flat combs (down to 7 dB) can be achieved, with mode RIN values of less than 0.3%, suitable for error-free transmission. These novel structures have been simulated using experimentally verified parameters and technologically feasible configurations.

Index Terms—Fourier-domain (FD) mode locking, integrated optoelectronics, mode-locked lasers, optoelectronic devices, semiconductor lasers.

I. INTRODUCTION

FUTURE demands on interconnect speeds to and on silicon chips run well into the hundreds of terabits per second regime. It can be estimated that this capacity cannot be realized using existing electronic interconnect technology, and hence, photonic interconnect technology is currently heavily investigated [1], [2]. For example, the Corona architecture proposed in [3] requires a 160-Tb/s total bandwidth and it is argued that this can only be achieved by using a dense wavelength-division multiplexed (WDM) approach, e.g., using 64 wavelength channels operating at 10 Gb/s. These developments require compact WDM sources that are able to generate multiple wavelengths on a frequency grid, i.e., having a fixed spacing. The number of channels and the maximum allowed footprint both call for integration of such sources on a single photonic chip.

On-chip WDM sources are commonly realized by monolithic integration of an array of single-mode lasers on an indiumphosphide (InP)-based chip [4]. Using hybrid integration, these sources can also be realized on silicon chips [5]. However, such a configuration requires wavelength lockers and stabilizers for every single-mode laser source, which adds significantly to the complexity and power consumption of the module.

Manuscript received October 15, 2010; revised December 29, 2010; accepted January 3, 2011. This work was supported in part by Intel, and in part by DARPA under Contract HR0011-10-C-0050.

The authors are with the University of California Santa Barbara, Santa Barbara, CA 93106 USA (e-mail: mheck@ece.ucsb.edu; bowers@ece.ucsb.edu).

Color versions of one or more of the figures in this paper are available online at <http://ieeexplore.ieee.org>.

Digital Object Identifier 10.1109/JSTQE.2011.2113371

A much more simple approach is to use a single laser source that can simultaneously generate a comb of frequencies, for example, a multimode laser or a mode-locked laser (MLL). The individual wavelengths in the mode comb can be separated using a demultiplexer, e.g., using ring filters or an arrayed waveguide grating. In such lasers, the spacing of the frequencies in the mode comb is determined by the cavity free spectral range (FSR). All the wavelengths of the mode comb of such a laser can be mapped to a dense wavelength division multiplexing (DWDM) frequency grid by tuning the cavity roundtrip time and by using only a single wavelength locker. Stable multimode and mode-locked sources have been realized in quantum well [6] and quantum dot gain materials operating at wavelengths around 1.3 μm [7] and 1.55 μm [8], and [9] have been successfully implemented in a WDM system [10]. The challenge with using these laser diodes is to achieve a suitable optical bandwidth to provide the required number of WDM channels and to have sufficiently low relative intensity noise (RIN) in the modes, which might increase due to mode partition noise [11].

In addition, we note that the optical output bandwidth of MLLs can be further increased using either passive [12], [13] or active [14], [15] nonlinear waveguide structures at the laser output. Alternatively, such waveguide structures can possibly be used to make integrated equivalents of the approach presented in [16], where a single-frequency laser source is externally modulated using a stable RF source. By nonlinear pulse compression, this modulated output can then be converted to broad bandwidth mode combs.

Recently, a novel laser mode-locking technique was shown, called Fourier-domain (FD) mode locking, where the frequency of the light is being modulated using a tunable optical bandpass filter [17]. Such lasers are different from both AM-MLLs, where the absorption or gain is modulated to achieve hybrid or active mode locking, and FM-MLLs, where the phase of the light is modulated using a phase of the FM modulator [18], [19]. These Fourier-domain mode-locked lasers (FD-MLLs) are able to generate large optical bandwidths close to 100 nm, but operate at a very small cavity free-spectral range (FSR) due to the long (fiber) cavity. These lasers are almost exclusively used for optical coherence tomography applications and although an FD-MLL with a 25-GHz comb was demonstrated [20], there have not been any studies on the application for data- and telecommunications.

In this study, we translate the concept of FD mode locking for the first time to integrated designs, effectively creating a whole new class of laser diodes. Integrated FD-MLLs will be strikingly different than the FD-MLLs presented in [17] because cavity roundtrip frequencies are typically in the order of

10–50 GHz as opposed to the 10–100 kHz range. This is due to the corresponding cavity lengths in the millimeter and kilometer range, respectively, i.e., six orders of magnitude difference. We present a feasibility study that focuses on two major points. First, we study the possibilities for mode-comb generation, with the emphasis on bandwidth, comb flatness, and mode RIN. Second, the practical feasibility of the proposed designs is discussed by comparing the requirements for the design with state of the art in photonic integrated technology on semiconductor platforms such as InP and silicon.

In the following, we first introduce the model that is used for the simulation of these devices in Section II. Then, we present different FD-MLL designs and their operation as a comb laser in Section III. This paper is concluded with a discussion about the validity and feasibility of the concept and possible improvements in Section IV.

II. MODEL

The theoretical model in this study is based on the work presented in [21] and [22]. We use parameters that are representative for the InP-based platform, since this is the material of choice for integrated lasers and semiconductor optical amplifiers (SOAs) operating around wavelengths of 1550 nm. This material system is well quantified and we use the experimental validation and parameter quantification presented in [14] of the model in [21] and [22]. We note that parameter values will differ for different epitaxial layer structures, quantum-well designs, and waveguide geometries, but the results presented in this study will be qualitatively representative for integrated circuits fabricated in any of these designs. We further note that these results are also representative for the hybrid silicon platform [23], since its SOAs are made from bonded InP-based epitaxial material. The commercial PICWAVE photonic circuit simulator is used to solve the time-domain travelling wave equations.

The complex field propagation is calculated for single transverse-mode and TE polarization operation, as is justified by a single-mode waveguide design and higher SOA gain for the TE than for TM mode. The waveguide geometry of [14] is used for the SOA, i.e., a $2\text{ }\mu\text{m}$ wide ridge waveguide, having a 120-nm bulk active region. Passive waveguides and phase modulators (PHMs) have a similar geometry, but without the bulk active layer, i.e., having a 500-nm InGaAsP transparent core. These geometries are used by PICWAVE to calculate confinement factor Γ , group velocity v_g , and spontaneous emission coupling constant β . PHMs are created by current injection of passive waveguide structures, as discussed later.

The SOA material gain as a function of wavelength λ is modeled using a single Lorentzian gain model and a linear gain g versus carrier density N approximation

$$g(\lambda, N) = \frac{a_N (N - N_{\text{tr}})}{1 + \varepsilon P} - a_N N_{\text{tr}} g_2 (\lambda - \lambda_0)^2 \quad (1)$$

where $a_N = 3 \times 10^{-20} \text{ m}^2$ is the differential gain, $N_{\text{tr}} = 0.3 \times 10^{18} \text{ cm}^{-3}$ the transparency carrier density, P the photon density, $\varepsilon = 10^{-15} \text{ cm}^3$ the nonlinear gain compression, which includes the effects of carrier heating and spectral hole burn-

ing, $\lambda_0 = 1550 \text{ nm}$ the wavelength corresponding to the gain peak, and $g_2 = 5000 \text{ }\mu\text{m}^2$ a parameter corresponding to the gain bandwidth.

The model is self-starting from a stochastic spontaneous emission noise source, with a bimolecular recombination constant $B = 10^{-10} \text{ cm}^3/\text{s}$. Two-photon absorption and nonlinear Kerr-effect are ignored, which is justified since ED-MLLs do not generate high-peak power pulses. The nonradiative carrier lifetime equals $\tau = 0.5 \text{ ns}$. The SOA passive loss is $\alpha_{\text{int}} = 20 \text{ cm}^{-1}$. Losses in passive waveguides are ignored; with minimum values of 0.5 dB/cm down to 0.2 dB/cm for InP- and silicon-based waveguides, respectively, these are insignificant as compared to α_{int} for (sub)millimeter-length cavities. Self-phase modulation is implemented by the linewidth enhancement factor $\alpha = 3$. The rate equations are solved by PICWAVE using a spatial discretization of $10 \text{ }\mu\text{m}$.

III. DESIGNS AND RESULTS

Using the model described in the previous section, we have simulated different integrated FD-MLL designs. We restrict ourselves to sinusoid driving signals, since in practice it will be very difficult or impossible to generate more complex electronic signals, e.g., a sawtooth function, at speeds of tens of gigahertz since the higher harmonics in the signal will fall outside of the electronic bandwidth of the components in the laser configuration.

A. Ring Modulator-Based Fundamental FD-MLL

In Fig. 1(a), a schematic of an FD-MLL with a filter based on a ring modulator is shown. The ring has a circumference of $50 \text{ }\mu\text{m}$, corresponding to an FSR of 1.7 THz. The ring modulator is placed in a loop mirror to avoid multiple passes of the optical field through the ring within one drive period. The total cavity length, including half of the loop mirror, is 1.6 mm, corresponding to a 25-GHz FSR. Light is coupled out through a semitransparent mirror [see the left-hand side (LHS) in Fig. 1(a)] with a reflectivity of 0.3, corresponding approximately to a cleaved or polished facet in an InP or silicon waveguide.

In the design, a tradeoff has to be made between mode spacing and PHM drive frequency. If the mode spacing becomes too dense, the output of the FD-MLL cannot be demultiplexed by, e.g., an arrayed waveguide grating or ring filters. On the other hand, a larger mode spacing corresponds to a shorter cavity, which in turn requires a higher drive frequency for the PHM. For silicon- and InP-based PHMs, bandwidths of over 40 GHz are commonly achieved [24]–[26]. Another tradeoff has to be made for the ring circumference. A smaller radius allows for a large FSR and hence a potentially larger optical bandwidth. On the other hand, the ring needs to be tuned over a significant part of its FSR, i.e., the phase needs to be shifted over at least π radians to utilize at least half of the FSR bandwidth. Ultrashort silicon modulators with lengths down to $100 \text{ }\mu\text{m}$ and with phase efficiency $V_\pi L$ of $0.36 \text{ V}\cdot\text{mm}$ have been reported in [27]. InP-based PHM efficiencies down to $1 \text{ V}\cdot\text{mm}$ have been shown [28]. So, our choice of $50\text{-}\mu\text{m}$ rings is at the limit of current technological feasibility.

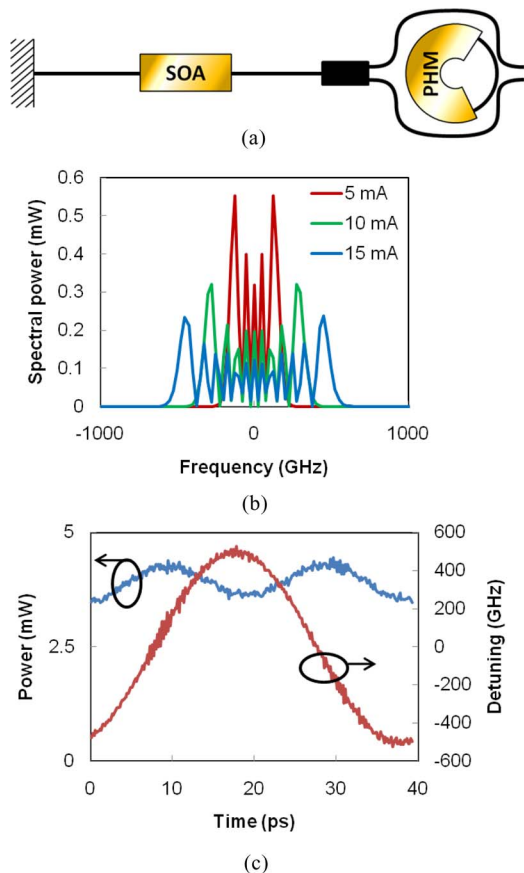


Fig. 1. (a) Schematic of the FD-MLL design. A 500- μm SOA is connected to a mirror ($R = 0.3$) and a loop mirror with a 50- μm circumference ring modulator. The PHM is used to modulate the transmission wavelength of the ring. The total Fabry-Pérot (FP) cavity length including half of the loopmirror is 1555 μm . (b) Output spectra for different PHM current amplitudes. Coupling factor to ring is 0.2 and $I_{\text{SOA}} = 50$ mA. Drive period for the PHM is 39.97 ps. Spectra are centered on $\lambda_0 = 1550$ nm. (c) Time domain output power (blue) and detuning or chirp (red) for the 15-mA PHM driving amplitude in (b).

In this study, PHMs have been simulated by current injection of a passive waveguide structure with a short carrier lifetime of 5 ps and having a linear index shift versus carrier density relation. The required injection currents and current amplitudes are chosen to reflect the state-of-the-art PHM performance and do not necessarily reflect the specific carrier and phase dynamics for an InP-based waveguide.

Fig. 1(b) shows the output spectra for driving the ring filter at 5, 10, and 15 mA amplitudes. The filter tuning is 42 GHz/mA, so this corresponds to ranges of ± 210 , ± 420 , and ± 630 GHz. It can be seen that the output bandwidth of the FD-MLL increases with increasing filter tuning range, as expected, and the widths of the spectra are 330 GHz, 650 GHz, and 1.0 THz, respectively. However, the spectra are not flat and show a modulation with dips of 13, 30, and 33 dB, respectively.

The time-domain signal corresponding to the 15-mA filter amplitude is shown in Fig. 1(c). The average output power is around 4 mW. There are two bumps in the spectrum, resulting from the sinusoid drive signal and the finite gain bandwidth. The chirp of the signal is significant, as can be expected from this type of laser, extending from -500 to 500 GHz, in agreement with

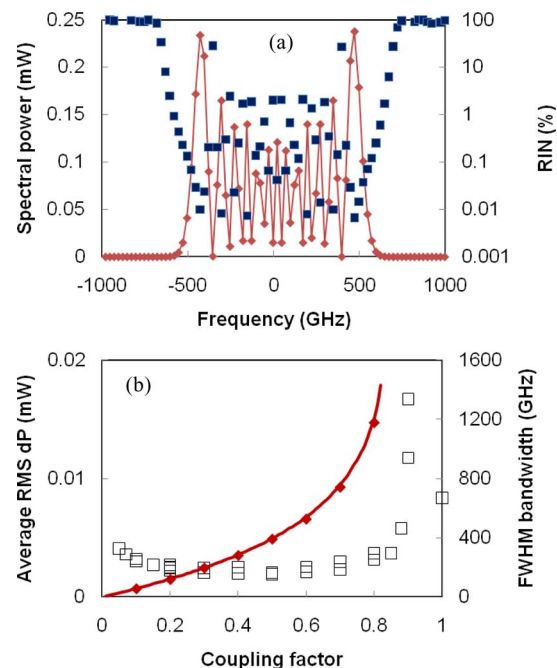


Fig. 2. (a) Spectral (mode) power (red) and RIN values of the modes (blue). Parameters are as in Fig. 1(b). (b) RMS mode power fluctuations dP (averaged over the mode comb) for different coupling factors to the ring (black squares). The ring transmission simulated numerically with PICWAVE and analytically according to [30] (red diamonds) is also shown.

the simulated spectral width of 1.0 THz as shown in Fig. 1(b). This sinusoid chirp profile of the field causes the modulation of the spectrum: the spectrum shows the interference between the fields that are generated during the frequency upsweep and downsweep of the filter, respectively.

In Fig. 2(a), the RIN values of the individual modes are shown, calculated according to [29]. Values have been calculated by first filtering the mode in the spectral domain and then transforming the filtered signal back to the time domain. The deviations from the average are then calculated over a time trace of 30 ns; hence, fluctuations in the order of 30 MHz up to around 4 THz (corresponding to the 10- μm discretization step size) are considered. As can be seen, the RIN of the modes has values up to 2% (range -500 to 500 GHz), with the exception of two low-power modes. There is a clear negative correlation between the mode power and the corresponding RIN value, where lower mode power leads to higher RIN values. Acceptable RIN values for error-free operation are around 0.4%, assuming that the RIN is the dominant mechanism contributing to the signal noise [8]. So concluding, it can be stated that the average RIN has to be brought down and the mode spectrum has to be flattened to avoid extremely large RIN values in the order of tens of percents. A second reason for flattening the spectrum is that when the laser is used as a WDM mode comb, less equalization is necessary in the circuit downstream. Both of these issues are separately addressed in the next two sections.

As a last point, we have studied the effect of the coupling of the waveguide to the ring [see Fig. 1(a)]. This coupling factor determines the width of the filter, ranging from, e.g., 200 GHz for a 0.3 coupling factor to a 1.2-THz width for a coupling factor

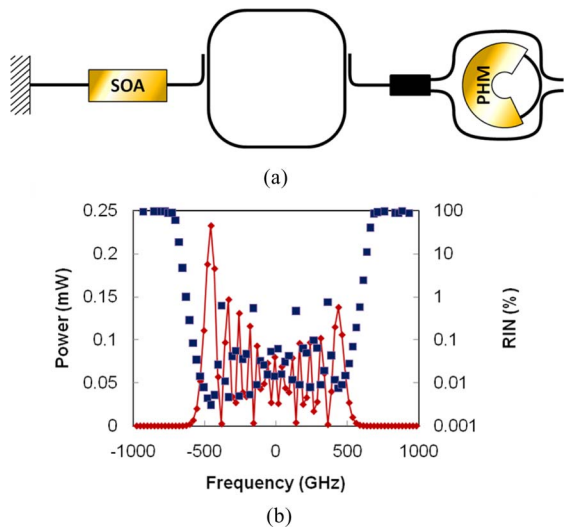


Fig. 3. (a) Schematic of the harmonically mode-locked FD-MLL. Total linear cavity has a 2.5-GHz FSR, including the loop-mirror, and the passive ring filter has a 25-GHz FSR. (b) Spectral (mode) power (red) and RIN values of the modes (blue). Both filters have coupling factors of 0.2. SOA injection current is 50 mA; PHM tuning current amplitude is 15 mA, similar to Fig. 1.

of 0.8. In Fig. 2(b), the average rms power fluctuations dP of the modes in the mode comb are plotted for coupling ratios ranging from 0.1 to 1.0, i.e., no filter. As can be seen, these values decrease until the coupling factor reaches a value of 0.5, corresponding to a 400-GHz filter width. It can be concluded that the FD locking mechanism is quite robust against variations in the width of the tunable filter.

B. Ring Modulator-Based Harmonic FD-MLL

To decrease the RIN of the comb lines, we investigate a configuration with a longer cavity. Increasing the cavity length will generally increase the coherence length of the modes and consequently the RIN, assuming no significant loss in the passive extended cavity [31]. Such configurations with long, low-loss cavities can be realized in, e.g., the hybrid silicon platform, where a sub-GHz MLL was reported [32].

In Fig. 3(a), the schematic of the harmonic FD-MLL can be seen. The linear cavity has a 2.5-GHz FSR, i.e., ten times as long as the configuration in Fig. 1(a). The tunable filter and the SOA are equal to the configuration in Fig. 1(a) and the cavity is assumed to be lossless. Harmonic mode locking is achieved by driving the PHM in the tunable filter at a frequency of 25 GHz. To minimize supermodes and the associated noise [33], a 25-GHz ring filter is placed inside the cavity [34]. Both this filter and the tunable filter have coupling factors of 0.2.

In Fig. 3(b), the mode spectrum for optimized operation is given. As can be seen, it looks similar to the spectrum shown in Fig. 2(a), with an equal width and supermodulation. This can be expected since the harmonic FD-MLL operates in a similar way as the fundamental FD-MLL in terms of pulse shaping. However, the RIN values of the harmonic FD-MLL are significantly lower, with values below 0.1% for most of the modes. The four low-power modes have RIN values of around

1%. So concluding, we have shown that the mode RIN values can be severely decreased by using harmonically mode-locked configurations.

C. Ring Modulator-Based Fundamental FD-MLL With Intracavity Modulator

The other problem that has to be solved is the supermodulation of the mode spectrum. First of all, the low-power modes have an increased RIN value [see Figs. 2(a) and 3(b)]. Second, for a WDM application the mode comb needs to be flat. Although it depends on the exact implementation, we expect that the supermodulation in the mode spectrum can certainly not exceed 10 dB.

As explained earlier, the supermodulation of the spectrum is caused by the interference between the fields that are generated during the frequency upsweep and downsweep of the ring filter. By suppressing one of these two parts of the field, it should be possible to get rid of the supermodulation. To achieve this, we propose the configuration that is shown in Fig. 4(a). In this configuration, a Mach-Zehnder-based amplitude modulator (MZM) is added to the cavity, which is driven with the same frequency as the filter. The MZM is placed at the mirror side to avoid multiple passes of the field. The output spectra of the FD-MLL as a function of the phase difference between the modulator and filter drive are shown in Fig. 4(b). It can be seen that spectral flatness and symmetry depend on the phase difference as can be expected, since the modulator carves out different parts of the sinusoidally chirped field [see Fig. 1(c)]. The most flat spectrum is observed around 330° phase difference and the corresponding time domain output is shown in Fig. 4(c). The pulse shows an upchirp and the downchirped part of the field is suppressed. As can be seen in Fig. 4(d), the spectrum shows only a 7-dB supermodulation and all modes have RIN values below 0.3% over the range -450 to 430 GHz, so it is clear that this configuration can flatten the mode comb and decrease the RIN extremities. In Fig. 4(d), the spectrum corresponding to 150° phase difference is also shown. The time domain output is a downchirped pulse (not shown). The spectrum shows a larger supermodulation (13 dB) than the 330° spectrum and is wider.

Low RIN values of below 0.3% correspond to narrow mode linewidths. In Fig. 5(a), a zoom-in of the central mode of the 330° phase difference spectrum is shown. By fitting a Lorentzian line-shape to the simulated spectrum, a 3-dB width of (15 ± 5) MHz is found. We note that the fitting accuracy of such linewidths is limited by the 25-MHz resolution of the spectrum, which is a limitation of the simulated time trace of 40 ns. In Fig. 5(b), all the 41 central modes of the spectrum are shown and overlaid. The modes have been normalized with respect to their power. All modes have a 3-dB width smaller than 25 MHz. This uniformity corresponds to the uniform RIN data as shown in Fig. 4(d). These values agree well with linewidth values reported for AM-MLLs [35].

As a practical point, we note that an electro-absorption modulator is also an option to replace the MZM. Furthermore, we note that the same RF source can be used for filter and modulator and only the relative phase (delay) between the two components has

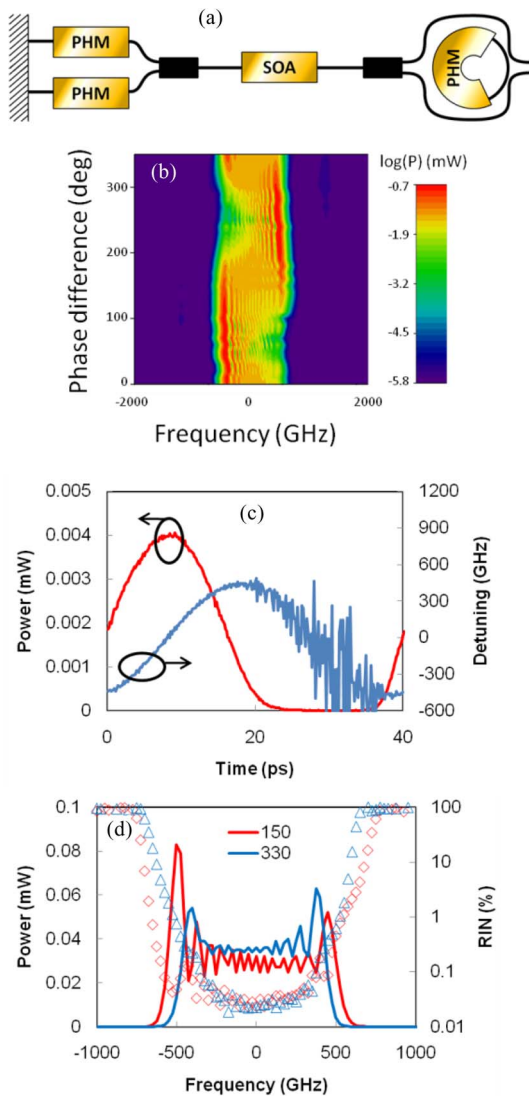


Fig. 4. (a) Schematic of the FD-MLL with and intracavity MZM. The PHMs in the MZM have a length of $500 \mu\text{m}$. A single PHM can be biased or both can be biased with opposite drive functions to increase efficiency. The other design parameters are as in Fig. 1(a). (b) Logarithmic plot of the output spectra as a function of the phase difference between the MZM and filter drive. (c) Power (red) and chirp (blue) of the time domain FD-MLL output for a phase difference of 330° . (d) Output spectra (lines) and RIN values (markers) for a phase difference of 150° (red) and 330° (blue). Further operation parameters are as in Fig. 1.

to be tuned. So, this design does not add too much complexity to the driving circuit as compared to the design in Fig. 1(a).

D. Mach-Zehnder Filter-Based FD-MLL

To alleviate requirements on the PHM length while increasing the filter bandwidth, an unbalanced Mach-Zehnder (MZ) filter can be considered. In this study, we ignore traveling wave effects, which is approximately valid if the PHM in the MZ filter is far smaller than the total cavity length. A schematic of the design is given in Fig. 6(a). The path length difference between the two arms of the MZ filter is $10 \mu\text{m}$, which leads to a

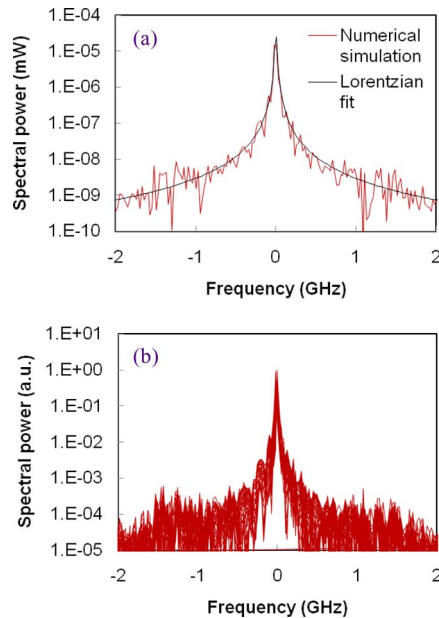


Fig. 5. (a) Optical spectrum (red) of the central mode (at -2 GHz) of the 330° phase difference spectrum in Fig. 4(d). The Lorentzian fit is also shown (black). (b) Normalized and overlaid spectra of the 41 central modes of the 330° spectrum. Resolution is around 25 MHz due to finite time-domain simulated trace.

4.25-THz FSR of the filter. By applying a bias to (one of) the PHMs, the MZ filter peak transmission is shifted, and hence, it operates as a wide-bandwidth optical filter with a large tuning range of 4.25 THz .

In Fig. 6(b) and (c), the simulated mode power spectra and corresponding RIN values are shown. As can be seen, the spectra show a severe supermodulation and corresponding RIN values are scattered over a large range. No clear optimum operating point can be identified.

In Fig. 7(a), spectra are shown for MZ filter drive current amplitudes of 5 , 10 , and 15 mA . The spectral width increases with increasing amplitude to 0.7 , 1.3 , and 1.8 THz , respectively. The RIN values are scattered over a larger range and have a higher value as observed for a ring-based filter in Fig. 2(a). This result shows that wide-bandwidth mode combs can be obtained with MZ filter-based configurations. In this particular case, the output consists of 72 comb lines, spaced at 25 GHz . The RIN is, however, high. To investigate this high RIN further, in Fig. 7(b) the ten central modes are shown for a PHM current amplitude of 10 mA . As can be seen, power exchange between modes takes place and adjacent modes show oscillations in antiphase with a periodicity of $\sim 6 \text{ ns}$. These oscillations add to the RIN and are responsible for the high RIN values. We note that these oscillations are unlike the periodic intensity fluctuations that are commonly observed in multimode semiconductor lasers, which show a switching sequence at periodicities on the order of $\sim 100 \text{ ns}$ [36]. In the feedback configuration of a ring filter, these oscillations are suppressed, but in the feedforward configuration of the MZ filter these oscillations dominate the RIN.

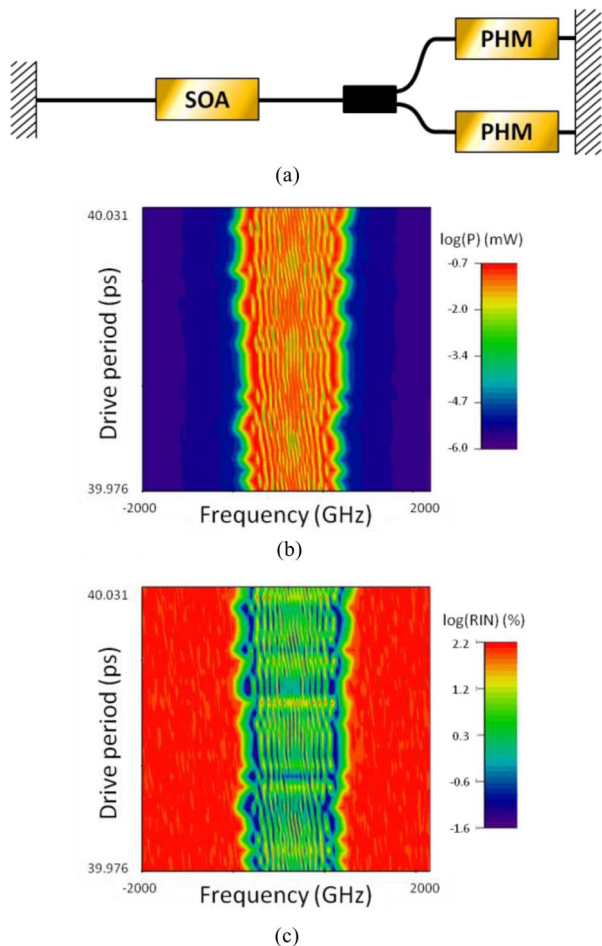


Fig. 6. (a) Schematic of the FD-MLL including an MZ-based filter. The MZ arms are 500 and 510 μm , respectively, and the mirrors in the filter [right-hand side (rhs)] are assumed to have a reflectivity of 1. The PHM drive amplitude is 10 mA. The 500- μm SOA parameters are as in Fig. 1. Mode power (b) and RIN (c) spectrum, color-coded in logarithmic scale.

E. Mach-Zehnder Filter-Based FD-MLL With Intracavity Modulator

Similarly to the configuration with a ring-resonator-based filter, we study the effect of an intracavity MZM for carving out part of the field. The configuration in Fig. 8(a) is used, where an MZM is used for the time-domain modulation and an unbalanced MZ filter is used to sweep the wavelength. The simulated spectra [see Fig. 8(b)] show a minimum RIN at 290° , as can be seen in Fig. 8(c). Fig. 8(d) shows the comparison with the design without MZM inside the cavity and it can be seen that the RIN extremities are significantly lowered and all RIN values fall within the 0.1–5% range. The flatness of the spectrum is improved to 9 dB as compared to 23 dB for the case without MZM.

IV. CONCLUSION

In summary, we have theoretically investigated a novel concept for an integrated mode-comb generator: an integrated FD-MLL. Our designs show four important features.

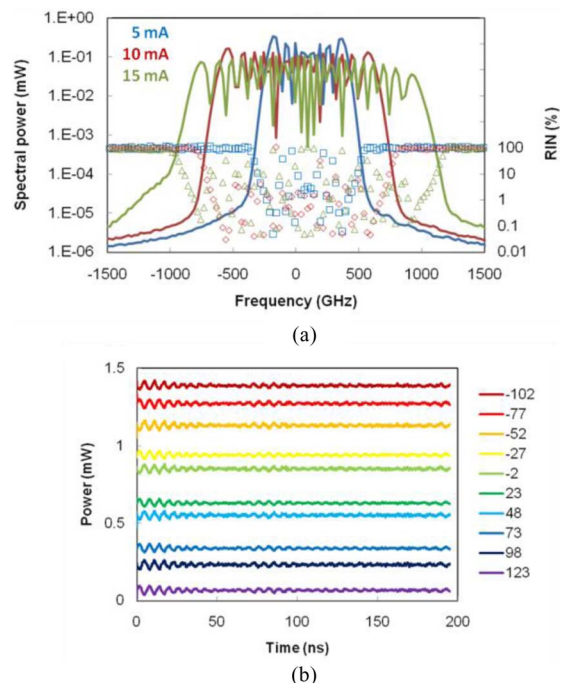


Fig. 7. (a) Mode power spectra (lines) and corresponding RIN values for different PHM drive current amplitudes, as indicated in the figure. Design and operation parameters are as in Fig. 6 and drive period is 40.01 ps. (b) Filtered modes at the frequencies indicated (in GHz). Modes have been offset by 0.15 mW for easy comparison. The modes correspond to the 10-mA plot in (a).

- 1) Comb widths that can be obtained using ring-resonator-based filters are in the order of 1 THz, mainly limited by the minimum size of the rings and the PHM efficiency. Wider combs can be generated using MZ-based filters, and we have shown that comb widths of 1.8 THz are feasible. Since the FD-MLLs in this work operate at 25 GHz, these widths are equivalent to 40 and 72 comb lines, respectively.
- 2) Due to the sinusoidal drive, the output fields have a sinusoidal chirp profile, which results in nonflat mode combs with a supermodulation on the spectrum in the order of 20–30 dB. We have introduced a novel design where we have added a modulator inside the cavity, driven at the same frequency as the filter. By tuning the relative phase of the drive signal between the filter and the modulator, we have decreased the supermodulation to only 7 dB. We note that these configurations actually operate in a hybrid AM/FD mode-locked state since pulse shaping and pulse narrowing take place due to the amplitude modulator, which is essentially different from the configuration presented in [37], where the pulse shaping is a result from the finite bandwidth of the gain medium.
- 3) We have shown that with an intracavity modulator RIN values can be uniform over the mode comb and have an upper limit of 0.3%. We have also shown that by using a harmonically mode-locked configuration, the RIN can be suppressed even further.
- 4) The proposed designs are practically feasible. The ring resonator-based configuration would require state-of-the-

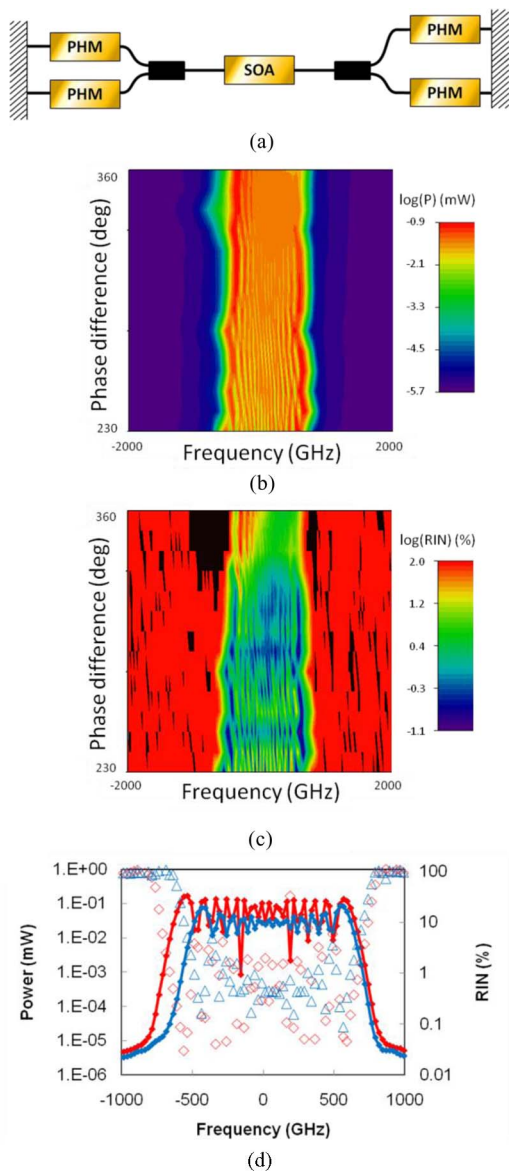


Fig. 8. (a) Schematic of the FD-MLL including an MZ-based filter and MZM. The filter arms are 500 and 510 μm , respectively, and the mirrors in the filter (rhs) are assumed to have a reflectivity of 1. The MZM arms are 500 μm and the mirror reflectivity (lhs) is 0.3. The PHM drive amplitude in the filter is 10 mA. The 500- μm SOA parameters are as in Fig. 1. Mode power (b) and RIN (c) spectrum, color-coded in logarithmic scale. (d) Comparison of mode power (line) and RIN (markers) without (red) and with MZM (blue).

art PHM specifications to obtain a 1-THz bandwidth, but the requirements on PHM performance are drastically alleviated when MZ-based configurations are used. The designs have been simulated using InP-based SOA parameters that have been experimentally verified.

These features have to be compared to the requirements for future interconnects. In [3], an architecture for 160 Tb/s total bandwidth is proposed that requires 64 channels operating at 10 Gb/s. This is well within reach of our proposed structure, which can achieve 72 comb lines, spaced at 25 GHz. The RIN level for error-free operation is around 0.4% [8], which is also within reach of this structure. To this we add that the SOA

structure we used in the model was not optimized for low-noise operation.

The optical output power of the FD-MLL should be increased though in future designs. Currently, we simulated average output levels of around 5 mW, which is a typical value for single mode laser diodes. For applications as a wide-band comb source, the average output power needs to be in the order of 0.8 W for the architecture proposed in [3]. By using an SOA with a large mode size, e.g., a slab-coupled optical waveguide amplifier, MLLs with 250 mW output have been achieved [38]. Also, extracavity flared SOAs can be used to boost the power. Extracavity SOAs can also be used to suppress RIN [39].

The electrical power consumption of the FD-MLL, counting only the electro-optical parts, is mainly determined by the power consumption of the SOA and the modulator. To get an estimate of the power consumption of the modulator, we use the value of 5 pJ/bit for the silicon modulators we referenced in our feasibility analysis [27]. This translates to about 0.1–0.2 W for 25-GHz modulators. The modulator can work virtually lossless, since it is operated in resonance with the optical field in the cavity, and hence, general laser optical efficiencies would apply for the FD-MLL. For example, in [40] a single-mode laser operating at 1.55 μm and with 0.86 W optical output is reported. The corresponding electrical power consumption is 7.2 W. This shows that at high-power operation the SOA power consumption dominates over the modulator and the FD-MLL efficiency can be in the order of state-of-the-art single-mode laser diodes.

Concluding, we can state that the integrated FD-MLL is a very promising approach to be used as a future comb source for Terabit/s DWDM interconnects. Besides this, because of the coherent nature of the comb, the FD-MLL can be used as a wide-band coherent source for optical code-division multiple access (OCDMA) [41], arbitrary waveform generation [42], ultrashort pulse generation [43], [44], and photonic analog-to-digital converters [45].

In this study, ring laser configurations have not been considered in detail, since initial simulations showed a strong effect of power exchange between the two counter propagating modes, which would complicate the analysis [46]. Furthermore, we did not consider Vernier-effect-based ring-resonator filters [47]. These filters can have an increased FSR while still having a relatively large radius and hence alleviated requirements for PHM length. The first simulations showed unstable operation, however, possibly due to the longer photon lifetime in the larger filters.

REFERENCES

- [1] D. A. B. Miller, "Device requirements for optical interconnects to silicon chips," *Proc. IEEE*, vol. 97, no. 7, pp. 1166–1185, Jul. 2009.
- [2] M. J. R. Heck, H.-W. Chen, A. W. Fang, B. R. Koch, D. Liang, H. Park, M. Sysak, and J. E. Bowers, "Hybrid Silicon photonics for optical interconnects," *IEEE J. Sel. Topics Quant. Electron.*, doi: 10.1109/JSTQE.2010.2051798 (forthcoming).

- [3] J. Ahn, M. Fiorentino, R. G. Beausoleil, N. Binkert, A. Davis, D. Fattal, N. P. Jouppi, M. McLaren, C. M. Santori, R. S. Schreiber, S. M. Spillane, D. Vantrease, and Q. Xu, "Devices and architectures for photonic chip-scale integration," *Appl. Phys. A.*, vol. 95, no. 4, pp. 989–997, Feb. 2009.
- [4] R. Nagarajan, M. Kato, J. Pleumeekers, P. Evans, D. Lambert, A. Chen, V. Dominic, A. Mathur, P. Chavarkar, M. Missey, A. Dentai, S. Hurtt, J. Bäck, R. Muthiah, S. Murthy, R. Salvatore, C. Joyner, J. Rossi, R. Schneider, M. Ziari, H.-S. Tsai, J. Bostak, M. Kauffman, S. Pennyacker, T. Butrie, M. Reffle, D. Mehuys, M. Mitchell, A. Nilsson, S. Grubb, F. Kish, and D. Welch, "Large-scale photonic integrated circuits for long-haul transmission and switching," *J. Opt. Netw.*, vol. 6, no. 2, pp. 102–111, 2007.
- [5] G. Roelkens, L. Liu, D. Liang, R. Jones, A. Fang, B. Koch, and J. E. Bowers, "III-V/silicon photonics for on-chip and intra-chip optical interconnects," *Laser Photon. Rev.*, vol. 9999, pp. 1–29, 2010.
- [6] Y. K. Chen, M. C. Wu, T. Tanbun-Ek, R. A. Logan, and M. A. Chin, "Multicolor single-wavelength sources generated by a monolithic colliding pulse mode-locked quantum well laser," *IEEE Trans. Photon. Techn. Lett.*, vol. 3, no. 11, pp. 971–973, Nov. 1991.
- [7] A. R. Kovsh, G. L. Wojcik, D. Yin, A. E. Gubenko, I. Krestnikov, S. S. Mikhlin, and D. A. Livshits, "Cost-effective DWDM optical interconnects enabled by quantum dot comb laser," in *Proc. Int. Soc. Opt. Eng. (SPIE) Photon. West*, 2010, vol. 7607.
- [8] Z. G. Lu, J. R. Liu, P. J. Poole, S. Raymond, P. J. Barrios, D. Poitras, G. Pakulski, X. P. Zhang, K. Hinzler, and T. J. Hall, "Low noise InAs/InP quantum dot C-band monolithic multiwavelength lasers for WDM-PONs," in *Proc. Opt. Fiber Commun. (OFC)*, 2009, pp. 1–3, Paper JWA27.
- [9] M. J. R. Heck, A. Renault, E. A. J. M. Bente, Y. S. Oei, M. K. Smit, K. S. E. Eikema, W. Ubachs, S. Anantathanasarn, and R. Nötzel, "Passively mode-locked 4.6 and 10.5 GHz quantum dot laser diodes around 1.55 μm with large operating regime," *IEEE J. Sel. Topics Quant. Electron.*, vol. 15, no. 3, pp. 634–643, May/Jun. 2009.
- [10] A. Akrouf, A. Shen, R. Brenot, F. Van Dijk, O. Legouezigou, F. Pommerau, F. Lelarge, A. Ramdane, and G.-H. Duan, "Error-free transmission of 8 WDM channels at 10 Gbit/s using comb generation in a quantum dash-based mode-locked laser," in *Proc. 34th Eur. Conf. Opt. Commun. (ECOC)*, Sep., 2008, pp. 21–25, Paper Th.3.D.4.
- [11] K. Haneda, M. Yoshida, H. Yokoyama, Y. Ogawa, and M. Nakazawa, "Measurements of longitudinal linewidth and relative intensity noise in ultrahigh-speed mode-locked semiconductor lasers," *Electron. Commun. Jpn. (Part II: Electron.)*, vol. 89, no. 2, pp. 28–36, Feb. 2006.
- [12] O. Boyraz, T. Indukuri, and B. Jalali, "Self-phase-modulation induced spectral broadening in silicon waveguides," *Opt. Exp.*, vol. 12, no. 5, pp. 829–834, 2004.
- [13] P. Koonath, D. R. Solli, and B. Jalali, "Continuum generation and carving on a silicon chip," *Appl. Phys. Lett.*, vol. 91, p. 061111, 2007.
- [14] M. J. R. Heck, E. A. J. M. Bente, Y. Barbarin, A. Fryda, H.-D. Jung, Y. S. Oei, R. Nötzel, D. Lenstra, and M. K. Smit, "Characterization of a monolithic concatenated SOA/SA waveguide device for picosecond pulse amplification and shaping," *IEEE J. Quant. Electron.*, vol. 44, no. 4, pp. 360–369, Apr. 2008.
- [15] M. J. R. Heck, E. A. J. M. Bente, Y. Barbarin, D. Lenstra, and M. K. Smit, "Monolithic semiconductor waveguide device concept for picosecond pulse amplification, isolation and spectral shaping," *IEEE J. Quant. Electron.*, vol. 43, no. 10, pp. 910–922, Oct. 2007.
- [16] L. Zhou, K. Kashiwagi, K. Okamoto, R. P. Scott, N. K. Fontaine, D. Ding, V. Akella, and S. J. B. Yoo, "Towards athermal optically-interconnected computing system using slotted silicon microring resonators and RF-photon comb generation," *Appl. Phys. A*, vol. 95, pp. 1101–1109, 2009.
- [17] R. Huber, M. Wojtkowski, and J. G. Fujimoto, "Fourier domain mode locking (FDML): A new laser operating regime and applications for optical coherence tomography," *Opt. Exp.*, vol. 14, no. 8, pp. 3225–3237, Apr. 2006.
- [18] L. F. Tiemeijer, P. I. Kuindersma, P. J. A. Thijs, and G. L. J. Rikken, "Passive FM locking in InGaAsP semiconductor-lasers," *IEEE J. Quant. Electron.*, vol. 25, no. 6, pp. 1385–1392, Jun. 1989.
- [19] A. E. Siegman, *Lasers*. Mill Valley, CA: Univ. Sci. Books, 1986, ch. 27.
- [20] T.-H. Tsai, C. Zhou, D. C. Adler, and J. G. Fujimoto, "Frequency comb swept lasers," *Opt. Exp.*, vol. 17, no. 23, pp. 21257–21270, Nov. 2009.
- [21] J. M. Tang and K. A. Shore, "Amplification of strong picosecond optical pulses in semiconductor optical amplifiers," *Proc. Inst. Elect. Eng.—Optoelectron.*, vol. 146, no. 1, pp. 45–50, Aug. 1999.
- [22] M. J. R. Heck, E. A. J. M. Bente, Y. Barbarin, D. Lenstra, and M. K. Smit, "Simulation and design of integrated femtosecond passively mode-locked semiconductor ring lasers including integrated passive pulse shaping components," *IEEE J. Sel. Top. Quant. Electron.*, vol. 12, no. 2, pp. 265–276, Mar./Apr. 2006.
- [23] H. Park, A. Fang, D. Liang, Y.-H. Kuo, H.-H. Chang, B. R. Koch, H.-W. Chen, M. N. Sysak, R. Jones, and J. E. Bowers, "Photonic integration on the hybrid silicon evanescent device platform," *Advances in Optic. Technol.*, vol. 2008, article 682978, pp. 1–17, Mar. 2008.
- [24] L. Liao, A. Liu, D. Rubin, J. Basak, Y. Chetrit, H. Nguyen, R. Cohen, N. Izhaky, and M. Paniccia, "40 Gbit/s silicon optical modulator for high-speed applications," *Electron. Lett.*, vol. 43, no. 22, pp. 1196–1197, Oct. 2007.
- [25] L. Zhang, J. Sinsky, D. Van Thourhout, N. Sauer, L. Stulz, A. Adamiecki, and S. Chandrasekhar, "Low-voltage high-speed travelling wave InGaAsP-InP phase modulator," *IEEE Photon. Techn. Lett.*, vol. 16, no. 8, pp. 1831–1833, Aug. 2004.
- [26] H. N. Klein, H. Chen, D. Hoffmann, S. Staroske, A. G. Steffan, and K.-O. Velthaus, "1.55- μm Mach-Zehnder modulators on InP for optical 40/80 Gbit/s transmission networks," in *Proc. Integr. Photon. Res. (IPR)*, Princeton, NJ, 2006, pp. 171–173.
- [27] W. M. J. Green, M. J. Rooks, L. Sekaric, and Y. A. Vlasov, "Ultra-compact, low RF power, 10 Gb/s silicon Mach-Zehnder modulator," *Opt. Exp.*, vol. 15, no. 25, p. 17106, Dec. 2007.
- [28] H. Ohe, H. Shimizu, and Y. Nakano, "InGaAlAs multiple-quantum-well optical phase modulators-based on carrier depletion," *IEEE Photon. Techn. Lett.*, vol. 19, no. 22, pp. 1816–1818, Nov. 2007.
- [29] R. Ju, P. S. Spencer, and K. A. Shore, "The relative intensity noise of a semiconductor laser subject to strong coherent optical feedback," *J. Opt. B: Quant. Semiclass. Opt.*, vol. 6, no. 8, pp. S775–S779, 2004.
- [30] E. J. Klein, "Densely integrated microring resonator-based components for fiber-to-the-home applications," Ph.D. dissertation, Faculty Electr. Eng., Math. Comput. Sci. (EEMCS), Univ. Twente, 2007, ch. 2.
- [31] T. Yilmaz, C. M. Depriest, A. Braun, J. H. Abeles, and P. J. Delfyett, Jr., "Noise in fundamental and harmonic modelocked semiconductor lasers: experiments and simulations," *IEEE J. Quant. Electron.*, vol. 39, no. 7, pp. 838–849, Jul. 2003.
- [32] M. J. R. Heck, M. Davenport, H. Park, D. J. Blumenthal, and J. E. Bowers, "Ultra-long cavity hybrid silicon mode-locked laser diode operating at 930 MHz," presented at the Optical Fiber Communication (OFC), San Diego, CA, pp. 21–25, Mar. 2010.
- [33] L. A. Jiang, "Ultralow-noise modelocked lasers," Ph.D. dissertation, Dept. Electr. Eng. Comput. Sci. MIT, Cambridge, MA, May 2002.
- [34] C. M. DePriest, T. Yilmaz, P. J. Delfyett, S. Etamad, A. Braun, and J. Abeles, "Ultralow noise and supermode suppression in an actively mode-locked external-cavity semiconductor diode ring laser," *Opt. Lett.*, vol. 27, no. 9, pp. 719–721, May 2002.
- [35] K. Haneda, M. Yoshida, M. Nakazawa, H. Yokoyama, and Y. Ogawa, "Linewidth and relative intensity noise measurements of longitudinal modes in ultrahigh-speed mode-locked laser diodes," *Opt. Lett.*, vol. 30, no. 9, pp. 1000–1002, May 2005.
- [36] A. M. Yacomotti, L. Furfaro, X. Hachair, F. Pedaci, M. Giudici, J. Tredicce, J. Javaloyes, S. Balle, E. A. Viktorov, and P. Mandel, "Dynamics of multimode semiconductor lasers," *Phys. rev. A*, vol. 69, p. 053816, 2004.
- [37] R. Huber, D. C. Adler, and J. G. Fujimoto, "Buffered Fourier domain mode locking: Unidirectional swept laser sources for optical coherence tomography imaging at 370,000 lines/s," *Opt. Lett.*, vol. 31, no. 20, pp. 2975–2977, Oct. 2006.
- [38] J. J. Plant, J. T. Gopinath, B. Chann, D. J. Ripin, R. K. Huang, and P. W. Juodawlkis, "250 mW, 1.5 μm monolithic passively mode-locked slab-coupled optical waveguide laser," *Opt. Lett.*, vol. 31, no. 2, pp. 223–225, Jan. 2006.
- [39] K. Sato and H. Toba, "Reduction of mode partition noise by using semiconductor optical amplifiers," in *Proc. IEEE 17th Int. Semicond. Laser Conf. Digest*, 2000, pp. 73–74.
- [40] J. J. Plant, P. W. Juodawlkis, R. K. Huang, J. P. Donnelly, L. J. Missaggia, and K. G. Ray, "1.5- μm InGaAsP-InP slab-coupled optical waveguide lasers," *IEEE Photon. Techn. Lett.*, vol. 17, no. 4, pp. 735–737, Apr. 2005.
- [41] R. G. Broeke, J. Cao, C. Ji, S.-W. Seo, Y. Du, N. K. Fontaine, J.-H. Baek, J. Yan, F. M. Soares, F. Olsson, S. Lourduodoss, A.-V. H. Pham, M. Shearn, A. Scherer, and S. J. B. Yoo, "Optical-CDMA in InP," *IEEE*

J. Sel. Top. Quant. Electron., vol. 13, no. 5, pp. 1497–1507, Sep./Oct. 2007.

- [42] N. K. Fontaine, R. P. Scott, J. Cao, A. Karalar, W. Jiang, K. Okamoto, J. P. Heritage, B. H. Kolner, and S. J. B. Yoo, “32 Phase X 32 amplitude optical arbitrary waveform generation,” *Opt. Lett.*, vol. 32, no. 7, pp. 865–867, Apr. 2007.
- [43] M. J. R. Heck, P. Muñoz, E. A. J. M. Bente, B. Tilma, Y. Barbarin, Y. S. Oei, R. Nötzel, D. Lenstra, and M. K. Smit, “Design, fabrication, and characterization of an InP-based tunable integrated optical pulse shaper,” *IEEE J. Quant. Electron.*, vol. 44, no. 4, pp. 370–377, Apr. 2008.
- [44] A. M. Weiner, “Femtosecond optical pulse shaping and processing,” *Prog. Quant. Electr.*, vol. 19, no. 3, pp. 161–237, 1995.
- [45] F. Coppinger, A. S. Bhushan, and B. Jalali, “Photonic time stretch and its application to analog-to-digital conversion,” *IEEE Trans. Microw. Theory Tech.*, vol. 47, no. 7, pp. 1309–1314, Jul. 1999.
- [46] E. A. J. M. Bente, Y. Barbarin, M. J. R. Heck, and M. K. Smit, “Modeling of Integrated Extended Cavity InP/InGaAsP Semiconductor Modelocked Ring Lasers,” *Opt. and Quant. Electron.*, vol. 40, no. 2–4, pp. 131–148, Mar. 2008.
- [47] D. H. Geuzebroek, E. J. Klein, H. Kelderman, F. S. Tan, D. J. W. Klunder, and A. Driessen, “Thermally tuneable, wide FSR switch-based on micro-ring resonators,” in *Proc. IEEE/LEOS Benelux Symp.*, 2002, pp. 155–158.



Martijn J. R. Heck (S'04–M'09) received the M.Sc. degree in applied physics and the Ph.D. degree from the Eindhoven University of Technology, Eindhoven, The Netherlands, in 2002 and 2008, respectively.

From 2007 to 2008, he was a Postdoctoral Researcher at the Communication Technology: Basic Research and Applications (COBRA) Research Institute, Eindhoven University of Technology, where he was engaged in the development of a technology platform for active–passive integration of photonic integrated circuits. From 2008 to 2009, he was with

the Laser Centre Vrije Universiteit, Amsterdam, The Netherlands, where he was involved in the development of integrated frequency combs generators. He is currently a Postdoctoral Researcher at the Department of Electrical Engineering, University of California, Santa Barbara, where he works on photonic integrated circuits based on the heterogeneous integration of silicon photonics with III/V materials.



John E. Bowers (F'93) received the M.S. and Ph.D. degrees from Stanford University, Menlo Park, CA.

He was with AT&T Bell Laboratories and Honeywell before joining the University of California, Santa Barbara (UCSB). He is currently the Fred Kavli Chair in Nanotechnology, the Director of the Institute for Energy Efficiency, and a Professor in the Department of Electrical and Computer Engineering, UCSB. He has published 8 book chapters, 450 journal papers, 700 conference papers, and received 52 patents.

Dr. Bowers and his coworkers received the EE Times Annual Creativity in Electronics (ACE) Award for most promising technology for the hybrid silicon laser in 2007. He is a member of the National Academy of Engineering, a Fellow of the OSA and the American Physical Society. He is a recipient of the OSA Holonyak Prize, the IEEE LEOS William Streifer Award, and the South Coast Business and Technology Entrepreneur of the Year Award.